Structure, dielectric and piezoelectric properties of donor doped PZT ceramics across the phase diagram

Shaji Karapuzha, A.; Kunnamkuzhakkal James, N.; Khanbareh, H.; van der Zwaag, S.; Groen, W. A.

DOI
10.1080/00150193.2016.1240571

Publication date
2016

Document Version
Final published version

Published in
Ferroelectrics

Ferroelectrics

ISSN: 0015-0193 (Print) 1563-5112 (Online) Journal homepage: http://www.tandfonline.com/loi/gfer20

Structure, dielectric and piezoelectric properties of donor doped PZT ceramics across the phase diagram

A. S. Karapuzha, N. K. James, H. Khanbareh, S. van der Zwaag & W. A. Groen

To cite this article: A. S. Karapuzha, N. K. James, H. Khanbareh, S. van der Zwaag & W. A. Groen (2016) Structure, dielectric and piezoelectric properties of donor doped PZT ceramics across the phase diagram, Ferroelectrics, 504:1, 160-171, DOI: 10.1080/00150193.2016.1240571

To link to this article: http://dx.doi.org/10.1080/00150193.2016.1240571

Published online: 21 Nov 2016.

FERROELECTRICS
2016, VOL. 504, 160–171
http://dx.doi.org/10.1080/00150193.2016.1240571

Taylor & Francis
Taylor & Francis Group

Structure, dielectric and piezoelectric properties of donor doped PZT ceramics across the phase diagram

A. S. Karapuzha[a], N. K. James[a], H. Khanbareh[a,b], S. van der Zwaag[a], and W. A. Groen[a,c]

[a]Novel Aerospace Materials Group, Faculty of Aerospace Engineering, Delft University of Technology, Delft, The Netherlands; [b]M2i, Delft, The Netherlands; [c]Holst Centre, TNO, Eindhoven, The Netherlands

ABSTRACT
The effects of Zr/Ti ratio on the dielectric and piezoelectric properties of the sintered $Pb(Zr_xTi_{(1-x)})_{0.99}Nb_{0.01}O_3$ piezoelectric ceramics across the entire range of phase diagram of the PZT solid solution was studied systematically. The materials were prepared by the conventional mixed oxide process. The phase purity and crystal structure of the calcined powders and sintered ceramics was analysed using X-ray diffraction. The microstructure of the sintered ceramics has been investigated using scanning electron microscopy. It is seen that even though there is a significant increase in dielectric constant (ε_r) and piezoelectric charge coefficient (d_{33}) at the PZT-52 (MPB) composition, the voltage sensitivity (g_{33}) of the PZT-0 (lead titanate) ceramics are higher than that of MPB.

ARTICLE HISTORY
Accepted 6 July 2016

KEYWORDS
PZT; morphotropic phase boundary; dielectric properties; piezoelectric properties

1. Introduction

Lead zirconium titanate, PZT, ceramics based on solid solutions of lead zirconate and lead titanate (PZT) are well known piezoelectric materials with widespread technological applications [1]. The compositional dependence of the perovskite structure and the electrical properties of PZT ceramics have been investigated extensively [1–3]. In this system rhombohedral and tetragonal phases coexist in a region known as the morphotropic boundary or MPB, which is a strong function of composition, $Pb(Zr_{0.52}Ti_{0.48})O_3$, and a weak function of temperature [1, 4]. In 1999, Noheda *et al.* [5] discovered a monoclinic phase, sandwiched between rhombohedral and tetragonal phases near the MPB in PZT ceramics and this monoclinic symmetry allows the polarization direction to continuously rotate in a plane and contributes to enhanced piezoelectric and dielectric properties at the MPB and nearby MPB region [1, 4]. Such PZT ceramics with compositions at MPB or near this region are much easier to pole and exhibit improved piezoelectric and dielectric properties compared to their rhombohedral and tetragonal counterparts. MPB based PZT ceramics and its compositionally modified variants with soft and hard dopants have been exploited in many sensor and transducer applications for their high electromechanical properties [6, 7]. Jaffe

CONTACT N. K. James nijeshkjames@gmail.com Novel Aerospace Materials Group, Faculty of Aerospace Engineering, Delft University of Technology, Kluyverweg 1, 2629 HS Delft, The Netherlands.

Color versions of one or more of the figures in the article can be found online at www.tandfonline.com/gfer.

et al., showed the dielectric and piezoelectric properties of PZT ceramics for Zr/Ti ratios ranging from 0.48 to 0.60 [1]. However, the piezoelectric and dielectric properties for the entire range of PZT compositions have not been methodically studied yet.

The present paper describes a study of the piezoelectric and dielectric properties for the complete solid solution of PZT ceramic $[Pb(Zr_xTi_{(1-x)})_{0.99}Nb_{0.01}O_3]$ with x = 0 to 0.80. Due to the antiferroelectric nature [8, 9], PZT compositions with $x > 0.80$ were not included in this investigation. The piezoelectric properties of PZT ceramics are improved by the addition of donor dopants, the popular one being Niobium (Nb) ions, resulting in the formation of Nb-doped PZT (PNZT) ceramics. The Nb^{5+} ions substitutes for the Zr^{4+}/Ti^{4+} ions at B-site and thereby promote domain wall motion in PZT ceramics [7]. Apart from providing superior piezoelectric and dielectric properties, Nb-oxide is also a good sintering aid for PZT-based materials resulting in higher density and smaller grain size with 1 mol % doping in the system [3]. Hence, 1 mol% Nb was added to the base system in order to make the poling and sintering process easier.

2. Experimental

A conventional solid state reaction method was used to synthesize the $Pb[Zr_xTi_{(1-x)}]_{0.99}Nb_{0.01}O_3$ ceramic powder with various Zr/Ti ratio with x varying from 0 to 0.80. The lead oxide (PbO), zirconia (ZrO_2), titania (TiO_2) and niobium pentoxide (Nb_2O_5), all having 99.9% purity were used as raw materials. The raw materials were weighed according to the stoichiometric proportions based on the desired ceramic composition. In order to attain homogeneity, the raw materials were thoroughly ball milled with 5-mm zirconium balls for 7 h in distilled water. The mixture was then dried in a hot air oven. The dried powder was calcined in a furnace at 750°C for 2 h using a heating rate of 2°C/min in order to initiate the formation of the perovskite phase. Phase formation was investigated with X-ray diffraction using a Bruker D8 diffractometer (Co Kα1, $\lambda = 1.78901$ Å). The powder was milled again as described above for 3 h. The dried powder was calcined again at 1150°C for 2 h at a heating rate of 2°C/min. The calcined powder was milled for 1 hr in order to obtain a particle size within the range of 2 to 4 μm. The presence of the tetragonal phase ($x \leq 0.5$), the rhombohedral phase ($x \geq 0.6$) and the coexistence of both phases at the morphotropic phase boundary ($x = 0.52$) was deduced from the X-ray diffraction patterns.

The calcined powders were then pressed into cylindrical pellets of 7 mm diameter. The compacts were sintered at 1250°C for 2 h in a bed of PZT powder in order to minimize the lead loss during the sintering process. The sintered ceramic discs were ground to a thickness of about 1 mm and its density was measured using Archimedes principle. Gold electrodes were applied on the ground faces by sputtering and the electroded ceramics were poled at 4 kV/mm at 100°C in silicon oil bath for 1 hr. The samples were then cooled to 30°C in the presence of the poling field and were allowed to age for 24 h before measuring the dielectric and piezoelectric properties. The dielectric constants of the ceramic disks were measured by means of the parallel plate capacitor method using an Agilent 4263B LCR meter at 1 V and 1 kHz. The piezoelectric charge constant (d_{33}) of the composites was measured using a high precision PM300 PiezoMeter System from Piezotest. The measurements were carried out at a static force of 10 N, a frequency of 110 Hz and a dynamic force of 0.25 N. The polarization measurements were performed at room temperature using the Precision Multiferroic Test System from Radiant Technologies for an applied field ranging from 1 kV/cm to 600 kV/cm and

at a frequency of 10 Hz. The strain hysteresis loop measurements were performed using a MTI photonic sensor (MTI-2100) in combination with the Precision Multiferroic Test System.

3. Results and discussion

3.1 Crystallographic phase analysis and microstructure characterization

XRD analysis

The room temperature X-ray diffraction patterns of the calcined $Pb[Zr_xTi_{(1-x)}]_{0.99}Nb_{0.01}O_3$ ceramics as a function of the Zr-fraction are shown in Fig. 1. The sharp and well-defined single phase diffraction peaks confirm the formation of the perovskite structure for all PZT powder compositions. The phases were identified by the analysis of the diffraction patterns within the two theta (2θ) range of 20° to 60°. For $x > 0.52$ the rhombohedral phase is observed. The splitting of (002) into (002) and (200) peaks at PZT-52 (MPB i.e. $x = 0.52$) indicates the morphotropic phase boundary (MPB) region, at which the co-existence of the tetragonal and rhombohedral phases is observed. The reason behind this splitting of reflections at MPB region can be attributed to the compositional fluctuations, leading to the coexistence of the rhombohedral and tetragonal phases [10–12]. It can also be seen that when Zr/Ti < 52/48, the diffraction patterns exhibit distinct (101) and (110) peaks at $2\theta = 36$ degree, which denotes the tetragonal structure of the ceramic powder.

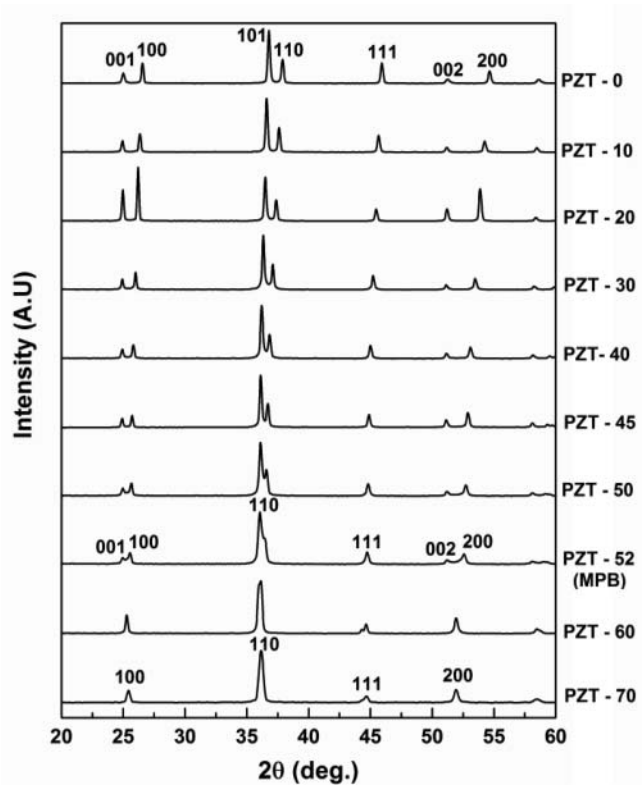

Figure 1. X-ray diffraction pattern of calcined $Pb[Zr_xTi_{(1-x)}]_{0.99}Nb_{0.01}O_3$ ceramic powder.

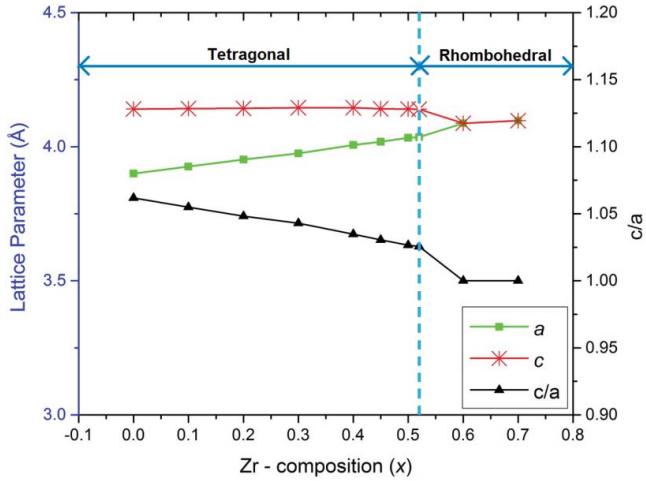

Figure 2. Lattice parameters and *c/a* ratio of calcined $Pb[Zr_xTi_{(1-x)}]_{0.99}Nb_{0.01}O_3$ ceramic powder.

Unit cell parameter

Figure 2 shows the variation of the lattice parameters '*a*' and '*c*' and *c/a* ratio as a function of the Zr mol. % of the ceramic powder. The *c*/a ratio for MPB composition of PZT (i.e. PZT-52) was found to be 1.025 whereas that of PZT-0 (i.e. lead titanate) was 1.062. Even though the lattice constant 'c' remains almost constant, an increase in lattice constant '*a*' is observed, leading to a reduction in the *c/a* ratio with increasing Zr content. This reduction in c/a ratio indicates that the tetragonality of PZT ceramics decreases with increase in Zr content. The values of the lattice parameters for a Zr/Ti ratio from 0.48 to 0.60 were found to be close to ones reported previously [13].

Particle size and morphology

Figure 3(a–c) shows the SEM micrographs of the calcined ceramic powder for Zr mol.% = 0 (tetragonal), 0.52 (MPB) and 0.80 (rhombohedral) respectively. The particle size of the calcined powder increases with the Zr content, which is in line with the results from particle size analysis. The calcined PZT-0 ceramic powder appears to have a spherical morphology whereas the other compositions possess polyhedral morphology.

Microstructure of sintered ceramics

Figure 4 (a) and (b) shows the SEM micrographs of sintered ceramics at 1250°C for Zr mol. % corresponding to 0 (PZT-0) and 0.52 (MPB) respectively. It can be seen that the MPB composition has a dense microstructure whereas PZT-0 with a high lead content cracked during sintering (see Fig. 4(c)). This cracking is the result of the large spontaneous strains and thermal expansion anisotropy associated with lead titanate ceramics upon cooling from sintering temperature through the cubic to the tetragonal phase transition at 490°C [14–16]. In addition, the formation of pyrochlore phase was not observed in case of both compositions as the presence of the non-ferroelectric pyrochlore phase will have a detrimental effect on the piezoelectric properties of the ceramics and hence formation of this phase is to be avoided [17]. The pyrochlore phase

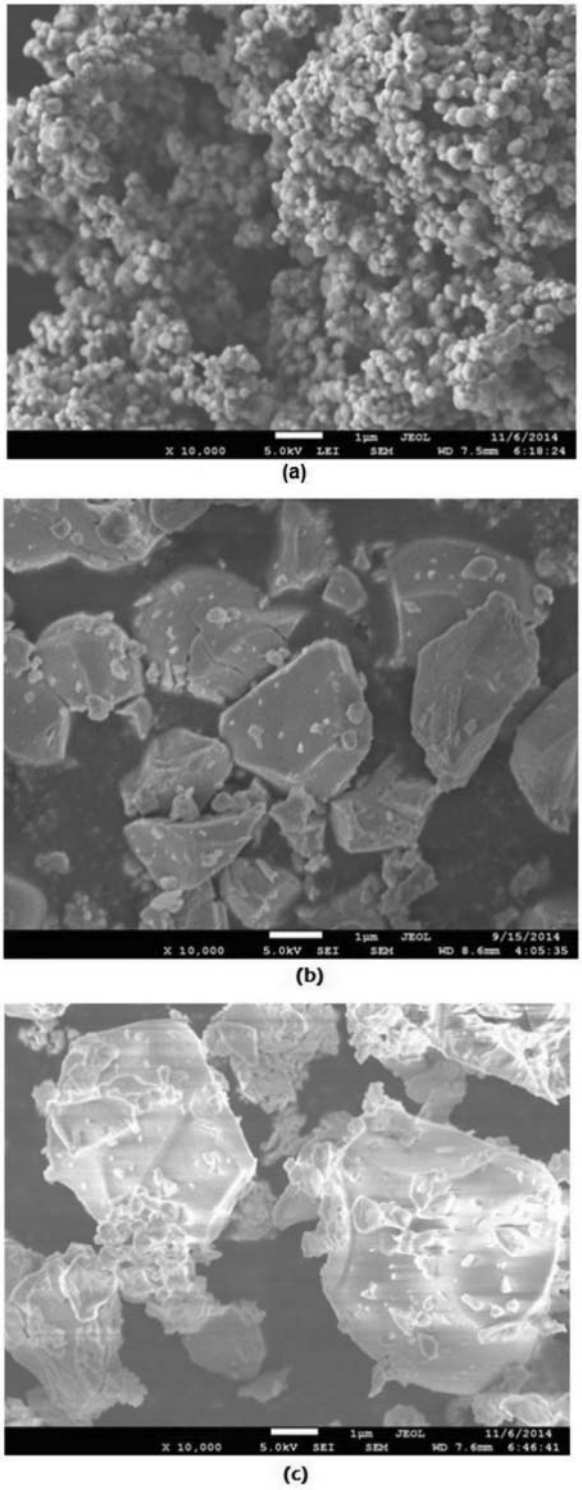

Figure 3. Microstructure of calcined ceramic powder for compositions corresponding to (a) PZT-0, (b) PZT-52 and (c) PZT-80 (i.e. $x = 0.80$)

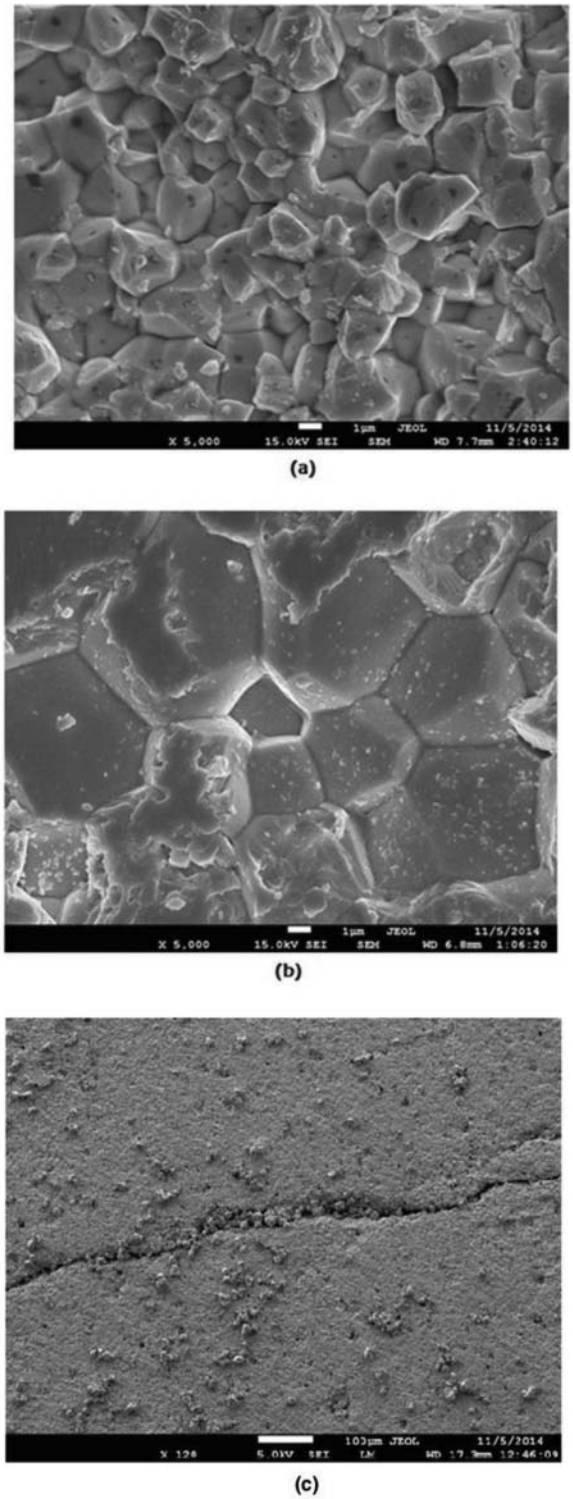

Figure 4. Microstructure of ceramic disks sintered at 1250°C for compositions corresponding to (a) PZT-0 (x = 0), (b) PZT-52 (x = 0.52) and (c) crack on surface of PZT-0 ceramics after sintering process.

Table 1. Density of the sintered $Pb(Zr_xTi_{(0.99-x)})Nb_{0.01}O_3$ ceramics for x ranging from 0 to 0.80.

Composition	Density (g/cm^3)
PZT-0 (PT)	7.12
PZT-10	7.18
PZT-20	7.20
PZT-30	7.25
PZT-40	7.30
PZT-45	7.35
PZT-50	7.41
PZT-52 (MPB)	7.49
PZT-60	7.41
PZT-70	7.41
PZT-80	7.39

was not observed in case of our calcined ceramic powders due to the two-stage calcination process followed [18, 19].

Table 1 shows the densities of the sintered $Pb(Zr_xTi_{(1-x)})_{0.99}Nb_{0.01}O_3$ ceramics measured using the Archimedes method. The densities of the sintered ceramics are in the range of 7.12 g/cm3 to 7.49 g/cm3 (90–93% of theoretical density) and are dependent on the Zr fraction. The relatively high density values indicate that the ceramic specimens prepared are eligible for electrical characterization.

3.2 Polarization measurements

Figure 5 shows the electric-field induced polarization hysteresis loop of $Pb(Zr_xTi_{(1-x)})_{0.99}Nb_{0.01}O_3$ ceramics, for x = 0, 0.52 (MPB) and 0.80, measured at room temperature at an applied field ranging from 4.5 to 7.5 kV/mm. The P-E hysteresis loop clearly shows that irrespective of the composition, polarization attains its saturation level at different electric fields. Furthermore, the P-E hysteresis displays significantly higher remnant

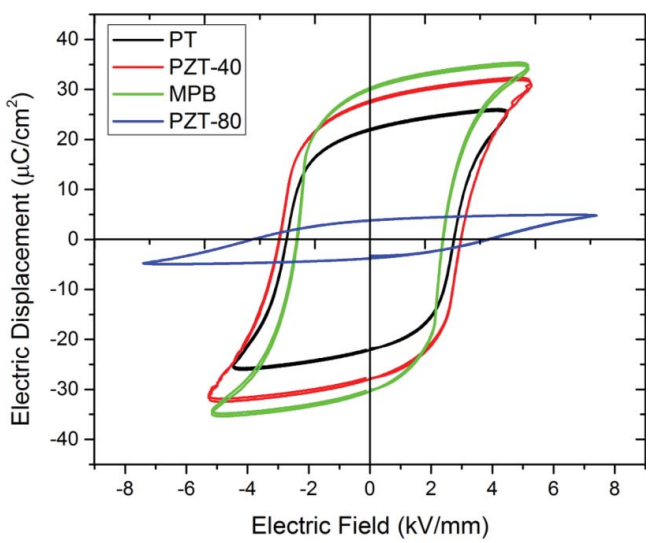

Figure 5. P-E Hysteresis loop for $Pb(Zr_xTi_{(1-x)})_{0.99}Nb_{0.01}O_3$ ceramics for x = 0 (PT), 0.40, 0.52 (MPB) and 0.80.

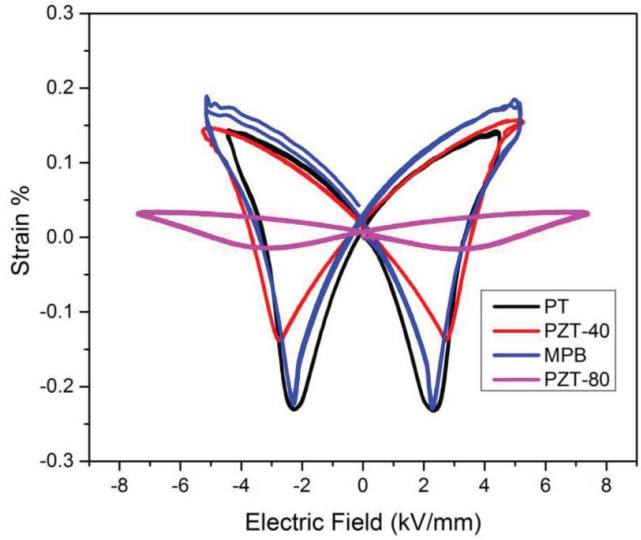

Figure 6. The electric-field induced strain curves of $Pb(Zr_xTi_{(1-x)})_{0.99}Nb_{0.01}O_3$ ceramics for x = 0 (PZT-0), 0.40, 0.52 (MPB) and 0.80.

polarization (P_r) for MPB ceramics with lower electric fields than that of its tetragonal and rhombohedral counter parts. The remanent polarization increases from lead titanate (PZT-0) with increasing Zr content till the MPB composition (PZT-52) and then decreases for Zr-rich compositions. The presence of 14 possible polarization states contributes to the highest remanent polarization at lower electric fields for the PZT ceramics at MPB.

Figure 6 shows the electric-field induced strain curves of $Pb(Zr_xTi_{(1-x)})_{0.99}Nb_{0.01}O_3$ ceramics, for x = 0, 0.52 (MPB) and 0.80, measured at a frequency of 10 Hz at room temperature. It can be seen that each composition exhibits the classical butterfly strain loops irrespective of their Zr/Ti ratio. The well-defined strain loop of PZT-0 and MPB ceramics suggests that these ceramics possess excellent actuation properties compared to that of the rhombohedral PZT ceramics. In general, the electric-field-induced strain in ceramics is caused by the domain switching, number of polarization states, electrostriction and the applied electric field. As a result, the MPB composition displays a maximum strain when rhombohedral and tetragonal phases coexist at the MPB, which in turn leads to enhanced polarization and piezoelectric properties [20]. Table 2 shows the remnant polarization (P_r), saturation polarization (P_s), coercive field (E_c) and piezoelectric charge coefficient (d_{33}) calculated from the hysteresis loops. The d_{33} coefficients were calculated from the slope of the linear portion of the strain hysteresis loop.

Table 2. Piezoelectric properties of $Pb(Zr_xTi_{(1-x)})_{0.99}Nb_{0.01}O_3$ ceramics for x = 0, 0.40, 0.52 (MPB) and 0.80.

Ceramics	$P_r(\mu C/cm^2)$	$P_s(\mu C/cm^2)$	E_c(kV/mm)	d_{33}*(pC/N)	d_{33}#(pC/N)
PZT-0 (PT)	22	26	2.7	83	53
PZT – 40	27.5	32	2.9	100	89
PZT-52 (MPB)	30	36	2.3	233	185
PZT – 80	3.8	5	4.2	20	14

*d_{33} measured from the butterfly loop; #d_{33} after polarization measurement (relaxation time = 24 h).

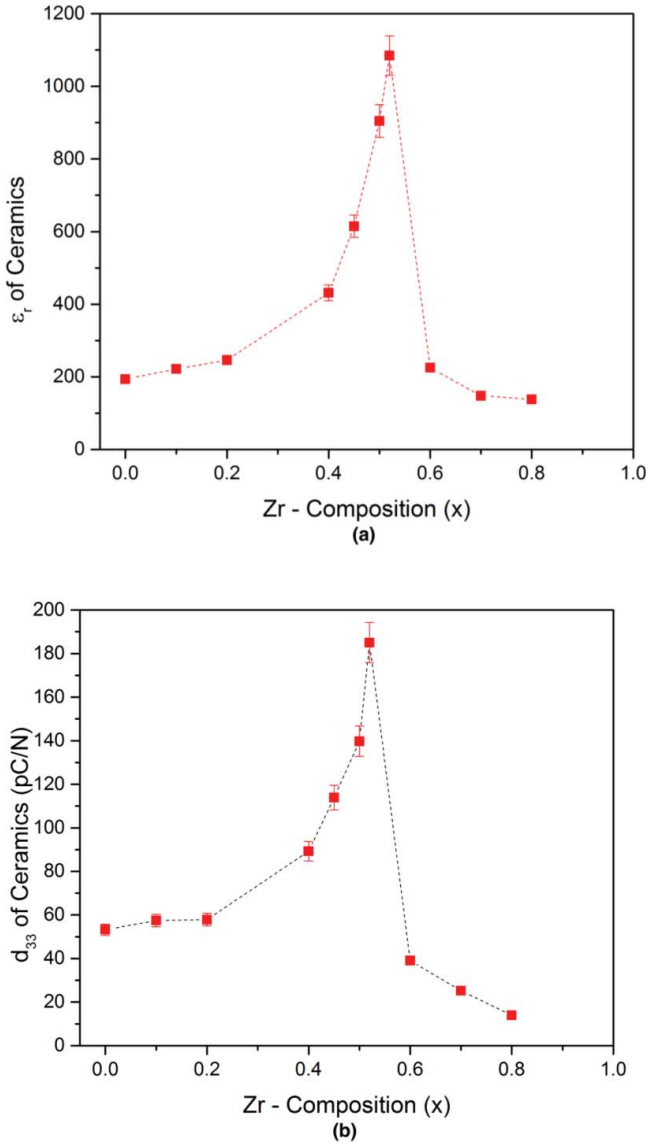

Figure 7. Variation of room temperature (a) dielectric constant (ε_r) and (b) piezoelectric charge constant (d_{33}) of $Pb[Zr_xTi_{(1-x)}]_{0.99}Nb_{0.01}O_3$ as a function of Zr mol.%.

Fig. 7(a) and 7(b) show the variation of dielectric constant and piezoelectric charge constant as a function of Zr mol.% respectively. Due to its large lattice anisotropy, a very high electric field and high temperature is required for poling the PZT-0 ceramics. However, it was impossible to pole PZT-0 ceramics at such severe poling conditions due to its low resistivity [14, 16].

As for the dielectric constant, the maximum value of the piezoelectric charge constant is also observed at MPB composition. The reason for this sharp increase in the dielectric and piezoelectric properties is attributed to the presence of 14 polarization states, originating from the co-existence of tetragonal and rhombohedral phases at MPB, which have nearly

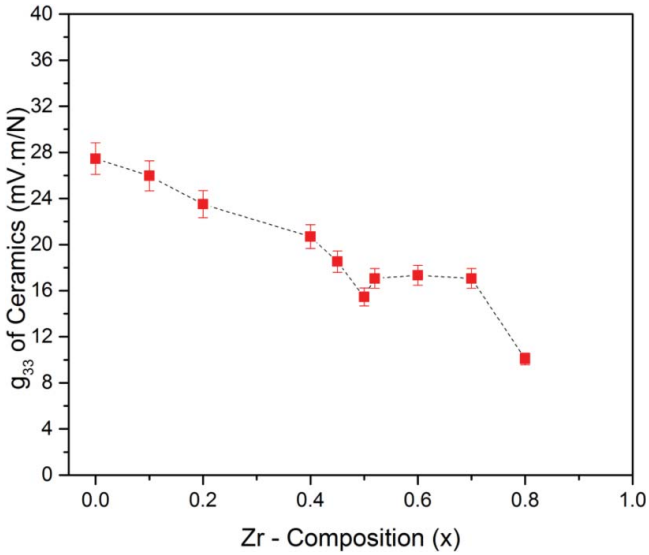

Figure 8. Variation of room temperature piezoelectric voltage coefficient (g_{33}) of $Pb[Zr_xTi_{(1-x)}]_{0.99}Nb_{0.01}O_3$ ceramics.

equivalent free energy. This provides a high polarization for MPB, which in turn favours strong dielectric and piezoelectric effects [21–23]. As mentioned previously, when $x > 0.52$, the ceramics contain only the rhombohedral phase whereas when $x < 0.52$, the ceramics contain the tetragonal phase. In either case, the number of domain variants is less than that of MPB composition, which in turn decreases the piezoelectric response of the ceramics. In addition, the porous nature of tetragonal ceramics also contributes to the decrease in piezoelectric charge constant since the porosity reduces the polarization per unit volume, which in turn reduces d_{33} [21, 24].

The piezoelectric voltage coefficient (g_{33}) of PZT ceramics as a function of the Zr content is shown in Fig. 8. It can be seen that the highest g_{33} is exhibited by $PbTiO_3$ (PZT-0) ceramics, in spite of its lower d_{33} than that of MPB ceramics. The significantly low dielectric constant of PZT-0 ($\varepsilon_r = 194$) compared to that of MPB (PZT-52) ceramics ($\varepsilon_r = 1085$) is responsible for this difference in the voltage coefficient. It is noteworthy that the piezoelectric voltage coefficients (g_{33}) increases towards the tetragonal field while it remains almost constant in the rhombohedral field until the antiferroelectric nature of the rhombohedral phase gains over the ferroelectric properties, after which the g_{33} drops down significantly.

4. Conclusions

The current work explored the piezoelectric and dielectric properties of $Pb(Zr_xTi_{(1-x)})_{0.99}Nb_{0.01}O_3$ piezoelectric ceramics for the range $x = 0$ to $x = 0.80$ covering the range from pure tetragonal ($x = 0$) to rhombohedral ($x = 0.80$) ceramics and including the MPB at $x = 0.52$. The highest dielectric and piezoelectric charge constants were obtained at the MPB composition. On the other hand, the piezoelectric voltage coefficient of PZT-0 (lead titanate) ceramics were significantly higher than that of MPB based ceramics but the poor sinterability and poling difficulties associated with

the lead titanate ceramics restrict its application in piezo devices. The higher piezoelectric voltage coefficient of PZT-0 ceramics can be used to develop highly voltage sensitive 0–3 ceramic-polymer composites as the ceramic granulates used in these composites are not sintered but calcined, thereby overcoming the sinterability and poling difficulties associated with its bulk ceramics.

Acknowledgments

This work was financially supported by the Smartmix funding program (Grant No. SMVA06071), as part of the program "Smart systems based on integrated Piezo." The authors gratefully acknowledge the support provided by Prof. de. D.M. de Leeuw and Dr. I. Katsouras of Max-Planck Institute for Polymer Research at Mainz for the hysteresis loop measurement.

Reference

1. B. Jaffe, W. R. Cook, and H. Jaffe, *Piezoelectric ceramics*, (1971).
2. E. Boucher, B. Guiffard, L. Lebrun, and D. Guyomar, "Effects of Zr/Ti ratio on structural, dielectric and piezoelectric properties of Mn-and (Mn, F)-doped lead zirconate titanate ceramics," *Ceramics international*, vol. **32**, pp. 479–485, (2006).
3. M. Pereira, A. Peixoto, and M. Gomes, "Effect of Nb doping on the microstructural and electrical properties of the PZT ceramics," *Journal of the European Ceramic Society*, vol. **21**, pp. 1353–1356, (2001).
4. A. Moulson, J. Herbert, "Piezoelectric ceramics," *Electroceramics: Materials, Properties, Applications, Second Edition*, pp. 339–410, (2003).
5. B. Noheda, D. Cox, G. Shirane, J. Gonzalo, L. Cross, and S.-E. Park, "A monoclinic ferroelectric phase in the Pb $(Zr_{1-x}Ti_x)O_3$ solid solution," *Applied Physics Letters*, vol. **74**, pp. 2059–2061, (1999).
6. J. F. Tressler, S. Alkoy, and R. E. Newnham, "Piezoelectric sensors and sensor materials," *Journal of Electroceramics*, vol. **2**, pp. 257–272, (1998).
7. S.-Y. Chu, T.-Y. Chen, I. T. Tsai, and W. Water, "Doping effects of Nb additives on the piezoelectric and dielectric properties of PZT ceramics and its application on SAW device," *Sensors and Actuators A: Physical*, vol. **113**, pp. 198–203, 7/5/2004.
8. X. Dai, J.-F. Li, and D. Viehland, "Weak ferroelectricity in antiferroelectric lead zirconate," *Physical Review B*, vol. **51**, pp. 2651, (1995).
9. X. Hao, J. Zhai, L. B. Kong, and Z. Xu, "A comprehensive review on the progress of lead zirconate-based antiferroelectric materials," *Progress in Materials Science*, vol. **63**, pp. 1–57, (2014).
10. A. Boutarfaia, "Investigations of co-existence region in lead zirconate-titanate solid solutions: X-ray diffraction studies," *Ceramics International*, vol. **26**, pp. 583–587, (2000).
11. A. Boutarfaia, C. Boudaren, A. Mousser, and S. Bouaoud, "Study of phase transition line of PZT ceramics by X-ray diffraction," *Ceramics international*, vol. **21**, pp. 391–394, (1995).
12. A. Boutarfaia, "Study of the solid state reaction and the morphotropic phase boundary in Pb(Zr, Ti)O_3-Pb $(Fe_{1/5}, Ni_{1/5}, Sb_{3/5})O_3$ ceramics," *Ceramics International*, vol. **27**, pp. 91–97, (2001).
13. S. Fushimi, T. Ikeda, "Phase Equilibrium in the System $PbO-TiO_2-ZrO_2$," *Journal of the American Ceramic Society*, vol. **50**, pp. 129–132, (1967).
14. A. Safari, E. K. Akdogan, *Piezoelectric and acoustic materials for transducer applications*. Springer, 2008.
15. S. Kim, M. c. Jun, and S. c. Hwang, "Preparation of Undoped Lead Titanate Ceramics via Sol—Gel Processing," *Journal of the American Ceramic Society*, vol. **82**, pp. 289–296, (1999).
16. T. Suwannasiri, A. Safari, "Effect of Rare—Earth Additives on Electromechanical Properties of Modified Lead Titanate Ceramics," *Journal of the American Ceramic Society*, vol. **76**, pp. 3155–3158, (1993).

17. N. Vittayakorn, G. Rujijanagul, T. Tunkasiri, X. Tan, and D. P. Cann, "Perovskite phase formation and ferroelectric properties of the lead nickel niobate–lead zinc niobate–lead zirconate titanate ternary system," *Journal of materials research*, vol. **18**, pp. 2882–2889, (2003).
18. D. S. Lee, C. W. Ahn, I. W. Kim, H. Y. Choi, Y. H. Jeong, J. S. Lee, et al., "The sintering behavior and piezoelectric properties of Pb $(Ni_{1/3}Nb_{2/3})$ O_3-$PbTiO_3$-$PbZrO_3$ ceramics using two-step calcination," *Journal of the Korean Physical Society*, vol. **42**, pp. 1215–1219, (2003).
19. R. Tipakontitikul, S. Ananta, "A modified two-stage mixed oxide synthetic route to lead zirconate titanate powders," *Materials Letters*, vol. **58**, pp. 449–454, (2004).
20. K. H. Yoon, H. R. Lee, "Electric-field-induced strain and piezoelectric properties near the morphotropic phase boundary of $Pb(Mg_{1/3}Nb_{2/3})O_3$ – $PbZrO_3$ – $PbTiO_3$ ceramics," *Journal of Applied Physics*, vol. **89**, pp. 3915–3919, (2001).
21. J. Holterman, P. Groen, *Piezoelectric Materials and Applications*. Apeldoorn, the Netherlands, Stichting Applied Piezo, 2012.
22. Y. Cao, G. Sheng, J. X. Zhang, S. Choudhury, Y. L. Li, C. A. Randall, et al., "Piezoelectric response of single-crystal $PbZr_{1-x}Ti_xO_3$ near morphotropic phase boundary predicted by phase-field simulation," *Applied Physics Letters*, vol. **97**, pp. 252904, (2010).
23. R. Waser, *Nanoelectronics and information technology*. John Wiley & Sons, 2012.
24. M.-C. Wang, M.-S. Huang, T.-S. Wong, and N.-C. Wu, "Sintering and piezoelectric properties of $Pb(Ni_{1/3}Sb_{2/3})O_3$-$PbZrO_3$-$PbTiO_3$ ceramics," *Journal of Materials Science*, vol. **37**, pp. 663–668, 2002/02/01 (2002).